

Carbonate-cemented stylolites and fractures in the Upper Jurassic limestones of the Eastern Iberian Range, Spain: A record of palaeofluids composition and thermal history

R. Marfil ^{a,*}, M.A. Caja ^b, M. Tsige ^c, I.S. Al-Aasm ^d, T. Martín-Crespo ^e, R. Salas ^b

^a*Dpto. de Petrología y Geoquímica, Facultad C.C. Geológicas, UCM, 28040 Madrid, Spain*

^b*Departament de Geoquímica, Petrologia i Prospecció Geològica, Facultat de Geologia, Universitat de Barcelona, 08028 Barcelona, Spain*

^c*Dpto. de Geodinámica, Facultad C.C. Geológicas, UCM, 28040 Madrid, Spain*

^d*Department of Earth Sciences, University of Windsor, Windsor, Ontario, Canada N9B 3P4*

^e*ESCET, Univ. Rey Juan Carlos, Edificio Departamental I, 28933 Madrid, Spain*

Abstract

Dolomite and calcite cements fill open stylolites, fractures and “pipe-shaped” structures related to faulting in Tithonian–Berriasian limestones of the Maestrat Basin in the Iberian Range (Spain). Due to the greater susceptibility of the dolomitised limestones to brittle fracturing during the Alpine tectonism, their location and distribution may have important implications for hydrocarbon prospectively within the studied region (Iberian Range). Three generations of structures were recognised (open stylolites, extensional fractures and faults) based on field observations, cross-cutting relationships and cement mineralogy. Petrographic, cathodoluminescence and geochemical analyses (electron microprobe, fluid inclusion, oxygen, carbon and strontium isotopes) of the carbonates helped unravel the origin and evolution of the fluids, from which these carbonates have been precipitated. These cements occur in the following structures:

- A) The first generation NNE trending fractures formed during the Late Eocene–Miocene compressional stage were filled by calcite cement ($\delta^{18}\text{O}$ VPDB -8.8‰ and $\delta^{13}\text{C}$ VPDB $+0.8$).
- B) The second generation represented by subvertical extensional fractures and the third generation by “pipe-shaped” structures, which are considered to be formed during the Miocene–Pliocene extensional stage, contain four carbonate cement phases: 1) isolated rhombic dolomites; 2) *saddle* dolomite with fluid inclusions characterised by high salinity (21.5 to 23.5 wt.% eq. NaCl), radiogenic Sr-enriched (0.70796 to 0.70857) in relation to the marine standard, high temperatures (T_h 110–155 °C) and low $\delta^{18}\text{O}$ values VPDB (-11.5‰ to -11.3‰); 3) calcitized *saddle* and rhombic dolomite with variable $\delta^{18}\text{O}$ VPDB -12.2‰ to -6.8‰ and $\delta^{13}\text{C}$ VPDB -4.4‰ to $+0.2\text{‰}$, and 4) two phases of calcite cements with moderate to high temperatures (T_h 110–125 °C, 15 to 19.7 wt.% eq. NaCl and 160–198 °C, 5.5 to 9.5 wt.%

eq. NaCl), low $\delta^{18}\text{O}$ VPDB values (-13.4‰ to -10‰) and positive carbon values ($\delta^{13}\text{C}$ VPDB $+0.1\text{‰}$ to $+1.8\text{‰}$). The diagenetic fluid is interpreted to be initially hot, saline, hydrothermal (temperature higher than the estimate of the ambient temperature) and Sr-enriched (0.70800). The dolomitisation event was followed by an input of meteoric water, which was related to the extensional stage. Finally, late calcite cement precipitated from fluids, which had initially moderate salinity and moderate to high temperature and later evolved to a lower temperature and higher salinity fluid (both Sr enriched). These fluids were probably derived from the progressive mixing of Late Triassic evaporitic brines with descending meteoric water that migrated via fractures during the Miocene–Pliocene Alpine extensional stage. Major vug-filling calcite cement is probably late in timing and related to hydrothermal karst associated with the “pipe-shaped” structure.

- C) Bed-parallel stylolites and subvertical extensional fractures, containing idiomorphic quartz crystals for which make it difficult to deduce the timing of its precipitation. Idiomorphic quartz has homogenisation temperatures of $140\text{--}180\text{ }^{\circ}\text{C}$ and salinities of 13.6 wt.% eq. NaCl. The high homogenisation temperature of this quartz and its association with dickite suggest precipitation from hydrothermal fluid.

Keywords: Fractures; Saddle dolomite; Calcite; Geofluids; Alpine deformation

1. Introduction

Dolomitisation associated with fractures is an important process that can indicate hydrothermal fluid flow, ore-forming brines, and the generation of reservoir porosity (Black et al., 1981; Knipe, 1993; Counter and Lowenstein, 1997). The occurrence of non-stratobound dolomitic bodies has been reported by several authors (Garreau et al., 1959; Black et al., 1981; Malone et al., 1996). These dolomitic bodies are referred to as “fault-controlled dolomitisation” (Machel and Mountjoy, 1986), “fracture-related dolomites” (Hurley and Budros, 1990) or “tectonic dolomites” (Harris, 1991). Dolomite bodies associated with fractures have different sizes, up to kilometers in length and several meters in width. These dolomite bodies can occur in the hanging wall or in the footwall of a tilted block and can show several shapes. The most typical is an elongated morphology (Jones, 1980; Black et al., 1981).

Most authors consider dolomite cementation associated with fractures to occur in the context of deep, hot-fluid circulation. Precipitation of carbonate cements in fault zones may be linked to: (a) compactional fluids (Machel and Mountjoy, 1986, 1987; Machel and Anderson, 1989); (b) hydrothermal fluids and brines (Machel and Mountjoy, 1986; Sellwood et al., 1989; Packard et al., 1990); (c) changes in fluid pressure associated with faulting events; (d) variations in the temperature of fluids during migration along fault

zones; (e) alterations in solubility arising from mixing of fluids of different composition, and (f) rock–fluid interactions resulting in dissolution–precipitation processes and diffusive mass transfer (Knipe, 1993).

In the Eastern part of the Mesozoic Iberian Range several dolomitisation events related to fractures have been reported: Zn–Pb Mississippi Valley-Type deposits are hosted by older dolostones and are related to the generation and circulation of ore-forming brines and dolomitising fluids during the earliest Tertiary (62.6 Ma) (Grandia et al., 1999, 2000, 2003; Nadal, 2001; Permanyer et al., 2001). Extensive dolomitisation event occurred as a result of hydrothermal fluids flow through fault systems during the earliest Cretaceous in the Eastern Iberian Range and the Linking Zone within the Catalan Coastal Range (Nadal, 2000, 2001). This dolomitisation event affected the emerged areas of the uppermost Jurassic–lowermost Cretaceous rocks during the Finibéricas regional unconformity (D3); hydrothermal events occur in the Neogene of the Catalan Coastal Range (Albert, 1976). Dolomites associated with fractures (Travé et al., 1998), barite and fluorite veins (Canals and Cardellach, 1996) have been linked to these hydrothermal fluids.

The objective of this paper is to investigate the relationship between carbonate cementation and fractures in order to find possible implications for hydrocarbon prospectively within the studied region (Iberian Range). Petrographic, isotopic and fluid inclusion analyses were performed to establish the ori-

gin and geochemical evolution of the fluids involved in dolomite and calcite cementation. The timing of fracture cementation is considered in the context of the structural history of the Alpine Orogeny based on the regional tectonic evolution of the Iberian Range.

2. Geological setting

The study area is located in the west Penyagolosa sub-basin in the outcrops of Cedrillas Fault (Teruel), Eastern Iberian Range, Spain (Fig. 1). The Penyagolosa sub-basin is one of seven sub-basins that became differentiated during the Late Jurassic–Early Cretaceous rifting event (latest Oxfordian–Middle Albian) in the Maestrat Basin (Salas and Guimerà, 1997; Salas et al., 2001).

The Maestrat Basin, containing a Mesozoic section of more than 5000 m, lies in the Eastern sector of the Iberian Range. The opening of the Alpine Tethys and Central Atlantic during the Late Jurassic initiated the

second intraplate Iberian rifting, with syn-rift subsidence beginning in the Maestrat Basin during the Late Oxfordian (Salas et al., 2001). This rift cycle 2 spanned the latest Oxfordian to middle Albian times. This rifting cycle can be subdivided into three discrete rifting pulses (Salas and Casas, 1993). The first pulse controlled the development of the Late Jurassic sequence in the Maestrat basin. The onset of rifting coincided with a significant rise in sea-level. Rapid subsidence of an array of tilted blocks resulted in the rapid drowning of up to 50 m thick shallow-water Oxfordian sponge-rich carbonates and the accumulation of up to 800 m thick Kimmeridgian deeper water carbonate rocks. Thin bedded lime-mudstones and sponge build-ups capped the crests of fault blocks (up to 500 m). These facies passed vertically into anoxic basinal marls (Ascla Formation) in the evolving hangingwall basins (up to 300 m). The Tithonian to Berriasian sequence is composed of assorted platform carbonates, deposited in a tidal flat (Pleta and Villar del Arzobispo formations) and as fringing oolitic-bio-

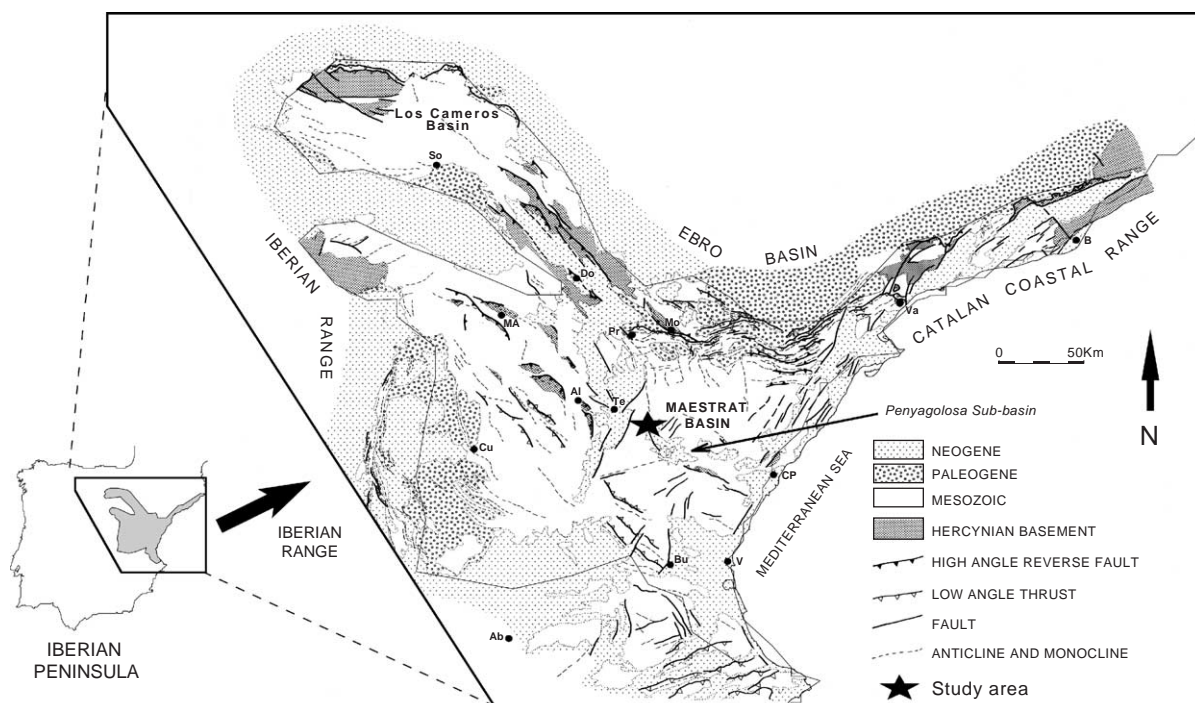


Fig. 1. Schematic map showing the location of the Iberian Range in the Iberian Peninsula and the general structure of the Iberian Range and the study area (modified from Salas et al., 2001).

clastic shoals, which graded basin-wards into hemipelagic *Calpionella* limestones, up to 1000 m thick (Higueruelas and Bovalar formations) (Salas et al., 2001).

The carbonate rocks investigated in this study are the Early Tithonian–Berriasian limestones (oncolithic packstone/grainstone) of the Bovalar Formation. This unit is composed of massive or thickly-bedded limestones with a high proportion of allochems, particularly oncolites and is bounded by two regional unconformities. In the study area the formation is approximately 850 m thick (Fig. 2, Aurell et al., 1994).

The tectonic history of the Penyalgosa sub-basin is related to the evolution of the Eastern Iberian Chain. A geotectonic model for the Alpine evolution of the Iberian Chain, consists of four stages: a Pre-Alpine syn-rift distension phase, two Alpine compression phases, with NE–SW and ESE–WNW shortening axis, respectively, and an essentially NE extensional tectonic phase with NE–SW dilatational axis (Álvaro et al., 1979; Simón, 1986; Salas and Casas, 1993). During the Neogene the tectonic regime changes as a consequence of the opening of the Valencia Trough. The area underwent extensional tectonics: 1) an ESE uniaxial extension and 2) a multidirectional extension regime (Simón, 1984, 1986). Most of these episodes are represented by macro- and micro-structures including stylolites, extensional fractures and faults affecting the Early Tithonian–Berriasian limestones. The micro-structures are commonly filled by several generations of carbonate cement.

3. Methods

This study includes an examination of the structural data, which affect the Bovalar Limestone Formation. We studied the paragenetic relationship between the fracture-filling carbonates and correlate these data with previous work where a qualitative chronological relationship of stress fields and fracturing at the meso- and macro-structural scale has been established (Álvaro et al., 1979; Simón, 1986; Salas and Casas, 1993; Liesa, 2000; Salas et al., 2001). The orientation, dipping, cross-cutting relations and filling of stylolites, extensional fractures and brittle shear zones were studied in the field.

Forty one samples of fracture-filling cement were collected. Double polished thin sections were stained with alizarin red S and potassium ferricyanide to distinguish Fe-rich and Fe-poor calcite and dolomite (Lindholm and Finkelman, 1972). Thin sections were examined by conventional light microscopy and cathodoluminescence, using a Technosyn 8200 MK4 unit fitted to a petrographic microscope. Samples were examined by X-ray diffraction to determine the mineral phases present.

Chemical analysis of the cements was performed on a Jeol JZA-8900M electron microprobe with four detectors. Operating conditions were: voltage 15 kV, current intensity 20 nA and electron beam diameter 5 µm. Detection limits were approximately 150 ppm for Ca, 100 ppm for Mg, 300 ppm for Fe, 250 ppm for

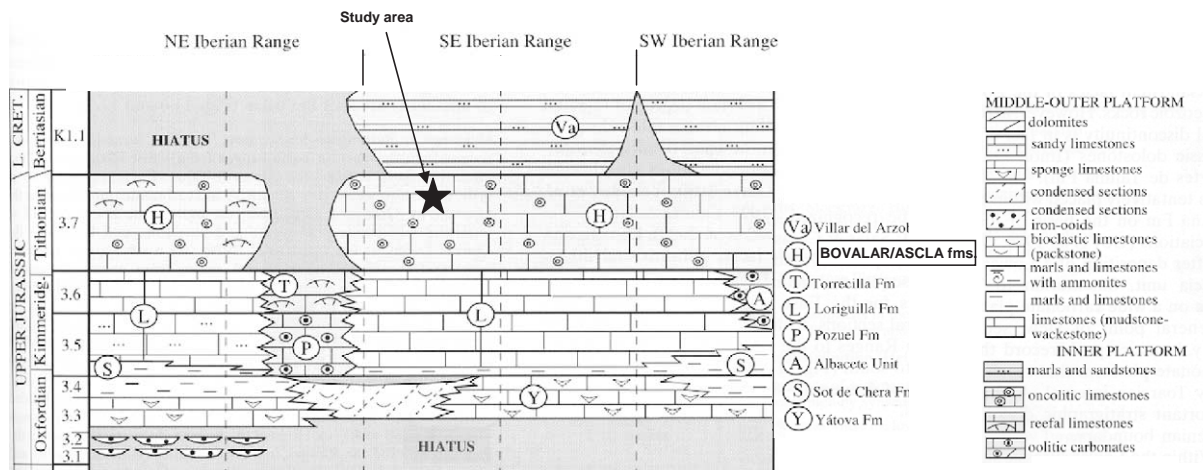


Fig. 2. Stratigraphy and facies distribution of the Upper Jurassic of the Iberian Range (modified from Aurell et al., 2002).

Mn, 250 ppm for Ba and 250 ppm for Sr. Double polished samples were coated with a carbon film. Results were standardised as 100% moles of CaCO_3 , MgCO_3 , FeCO_3 and MnCO_3 .

Fluid inclusion microthermometry was carried out on a Linkam THMSG 600 heating-cooling stage (which admits a temperature range of -196 to 600°C) attached to an Olympus BH-2 microscope equipped with a long focal distance lens ($80\times$). The apparatus was calibrated at low temperature by inclusion of pure CO_2 in topaz (-56.6°C) and synthetic inclusions of pure water in quartz (0.015°C), and at high temperature by known standard melting temperatures provided by Merck.

Stable oxygen and carbon isotope ratios were measured from 20 samples of calcite and dolomite extracted from rock sections using a microdrill attached to a binocular microscope. The samples were reacted for four hours with pure phosphoric acid in a vacuum, at 25°C for calcite and 50°C for dolomite (Al-Aasm et al., 1990). The CO_2 produced was analysed in a Delta-Plus mass spectrometer. C and O isotope ratios are given in permil with respect to the Vienna Pee Dee Belemnite (VPDB) standard. Precision was better than 0.05‰ for both isotopes. Sr isotopes were analysed from 13 calcite and dolomite samples using a VG Sector 54 mass spectrometer. The standard used was NBS-987 and the 2σ value for each measurement was lower than 0.00003 .

4. Results

4.1. Studied structures

Carbonate rocks of the Bovalar Formation display various structural features such as extensional fractures, stylolites and faults. Three generations of structural features were recognised. The first generation consists of two major sets of stylolites (Fig. 3-A). The first set is represented by vertical stylolites (Ve1) with a sub-horizontal orientation of the wavelength peaks, trending ESE. These vertical stylolites are interpreted as having a tectonic origin and are suggested to have formed during the ESE, post-rift compression phase (Late Eocene–Miocene), which affected this sector of the Iberian Range (Álvaro et al., 1979; Simón, 1986; Liesa, 2000; Capote et al.,

2002). The second set consists of well developed bed-parallel stylolites (BPSe2), with different morphology from that of the vertical stylolites. Peaks are roughly subvertical, predominantly columnar. The bed-parallel stylolites (BPSe2) crosscut the vertical stylolites (Ve1) indicating that BPSe2 postdate Ve1. The BPSe2 are suggested to have formed during the late post-rift NE trending extensional tectonic phase (Simón, 1986; Salas et al., 2001). This deformation event has started at the beginning of the Neogene in the Iberian Range (Simón, 1986; Salas et al., 2001). Some of these stylolites are up to 3 mm wide and filled by calcite and dolomite cements (Fig. 3-B).

The second generation of fractures consists of subvertical carbonate cemented fractures. Fracture width is variable, ranging from few mm to a maximum of 50 mm, and the fracture is filled with calcite and dolomite cements. The average length of the subvertical fractures is on the order between from 10 to 20 m and the spacing ranges from medium to wide (between 1 and 3 m). Structural data of the measured fractures are recorded in a stereogram (Fig. 4) and show two principal orientations, NNE (g1) and SE–SSE (g2) (Fig. 3-C). The fractures striking NNE (g1) are filled by white carbonate cement (dolomite and calcite) while the SE–SSE (g2) are filled by a brownish carbonate cement. Geometry of the fractures is somewhat complex to determine the chronological relationship between them. However, the white calcite cemented fractures (g1) are cut by and hence predate the brownish carbonate (dolomite and calcite) filled fractures (g2). Like wise, the second-generation fractures (g2) cross-cut the bed-parallel stylolites (BPSe2), and are cut by the bed-parallel stylolites indicating that they are synchronous (Fig. 3-D and E).

The third generation of fractures consists of several subvertical faults, predominantly NE–SW and NW–SE trending, with considerable dextral strike-slip component (Fig. 3-F and Fig. 4). These faults cut the bed-parallel stylolites (BPSe2). Some of the faults contain fibrous calcite with semi-horizontal striae, rock breccias and fault-gouge (Figs. 3-F and 5-A). The fillings are brecciated with major chemical alteration linked to the circulation of fluids, and clasts different from the immediate neighboring fractures and host rock (Fig. 5-B, C and D).

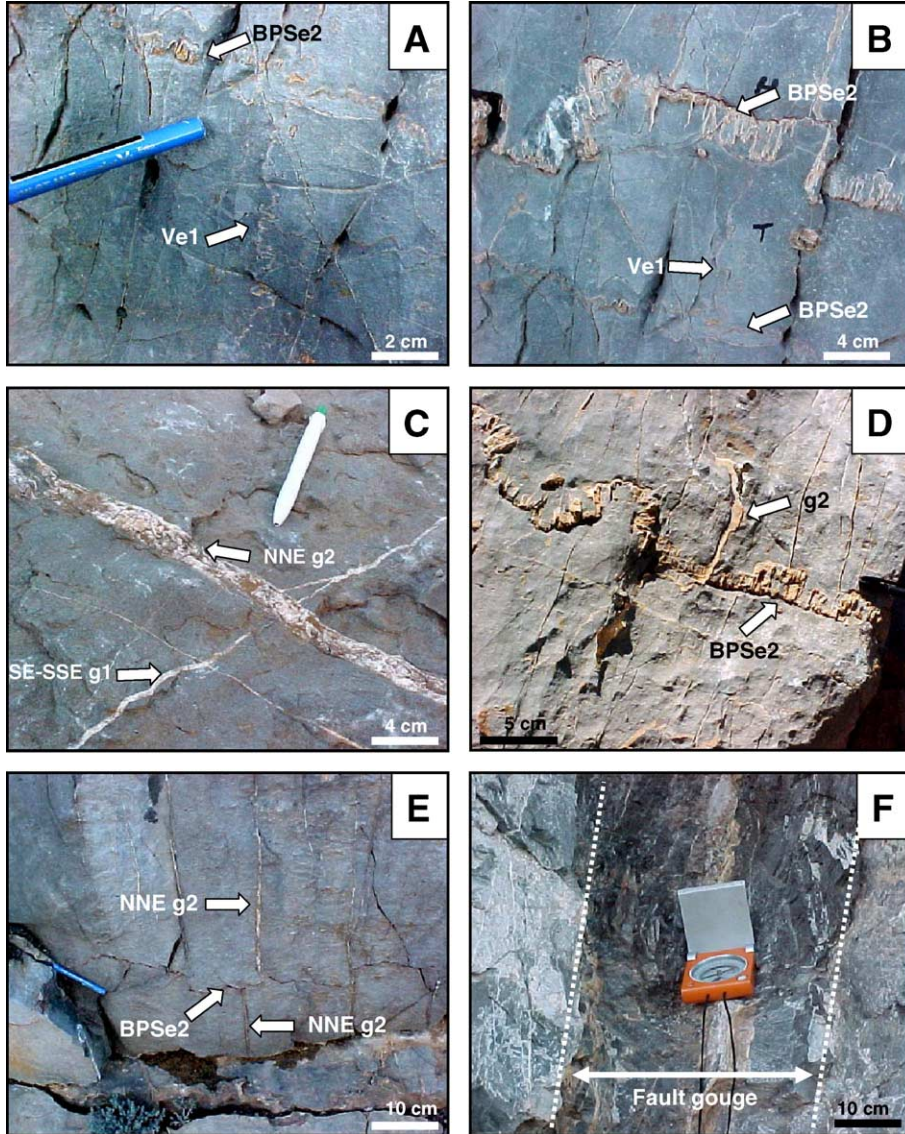


Fig. 3. Cross-section macroscopic view of the studied micro-structures. (A) Two major sets of stylolites: Vertical stylolites (Ve1) and bed-parallel stylolites (BPSe2). (B) Bed-parallel stylolite (BPSe2) filled by carbonate cement. Note the occurrence of scarce vertical stylolites (Ve1). (C) Subvertical carbonate cemented fractures with two principal orientations, NNE (g1) and SE-SSE (g2). (D) and (E) Fractures (g2) cross-cut the bed-parallel stylolites (BPSe2), but itself cut by the bed-parallel stylolites indicating that they are synchronous. (F) Subvertical brittle fault containing fault-gouge.

4.2. Petrology and geochemistry

The paragenetic sequence (Table 1) shows the formation of two generations of fractures, (g1) and (g2), and the “pipe-shaped” fault related structure include: calcite phase, two dolomite phases, calcitized dolomite phase and a final calcite phase.

4.2.1. Calcite cements in the first generation of fractures (g1)

Calcite crystals, which are in contact with the host rock and occlude the first generation of fractures (g1), show a rhombic habit with curved faces, and are clouded by Fe-oxide inclusions (Fig. 6-A). Under cathodoluminescence, this calcite is bright yellow lumines-

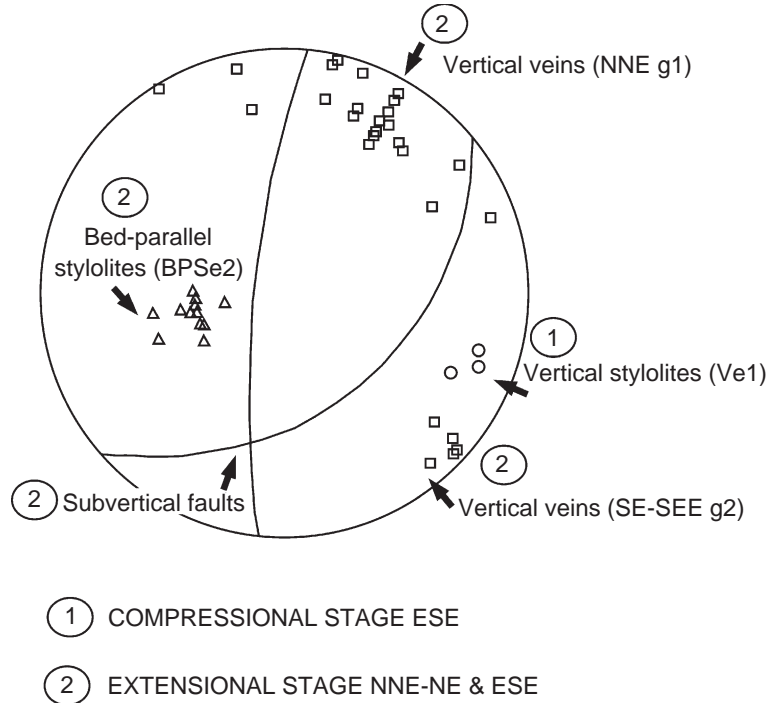


Fig. 4. Stereographic projection of the different fractures which affect the studied carbonate rocks. It shows that there exists three main fracture generation which correspond to different stress orientation which are associated with different tectonic regimes in the Iberian Chain.

cent (Fig. 6-B), and shows large, highly elongated to fibrous crystals ($<1\ \mu\text{m}$ in width). This calcite is characterised by alternating light and non-luminescent bands, showing a slightly undulatory extinction and a brownish orange and bright yellow luminescence (Fig. 6-B). The chemical composition of the crystals is $(\text{Ca}_{0.987}\text{Mg}_{0.011}\text{Fe}_{0.002}\text{Mn}_0)\text{CO}_3$ ($n=29$). Sr concentration ranges from undetectable to 837 ppm and the Ba content from undetectable to 1048 ppm (Fig. 7). The $\delta^{18}\text{O}$ value is -8.8‰ and $\delta^{13}\text{C}$ value is $+0.8\text{‰}$ (Fig. 8).

Occasionally, the curved calcite crystals (dedolomite) in contact with the host rock contain Fe-oxide inclusions and small scattered patches of dolomite. These dolomite crystals are too small in size to be analysed by electron microprobe.

4.2.2. Carbonate cements in second generation of fractures (g2) and “pipe-shaped” structure

Four generations of cement have been identified in the (g2) fractures and in the “pipe-shaped” structure (Table 1):

4.2.2.1. Rhombic dolomite. This phase consists of small, isolated dolomite rhombs (up to $800\ \mu\text{m}$ in size;

Fig. 6-C), which are usually in contact with the host rock (Fig. 6-D). Under cathodoluminescence, individual crystals display a non-luminescent core with an outer calcitised zone showing thin alternating bright-orange and bright-yellow bands. The chemical composition of the rhombic dolomite is $(\text{Ca}_{0.548}\text{Mg}_{0.415}\text{Fe}_{0.036}\text{Mn}_0)(\text{CO}_3)_2$ ($n=11$). The difficulty in isolating the small rhombs for proper sampling prevented isotopic analyses of this carbonate phase.

4.2.2.2. Saddle dolomite. Saddle dolomite crystals line fractures in highly disrupted and brecciated oncogenic limestones (Fig. 6-E and F). The mineral also appears as replacement of the carbonate host rock in the “pipe-shaped” structure (Fig. 5-B, C and D). The replacement zone is approximately 6 m in the vertical dimension and about 2 to 4 m in the horizontally dimension (Fig. 5-B). In both cases, the saddle dolomite crystals exhibits curved faces (Fig. 6-F), sweeping extinction, and dull brown to dull luminescence. The chemical composition of this dolomite is $(\text{Ca}_{0.537}\text{Mg}_{0.448}\text{Fe}_{0.015}\text{Mn}_0)(\text{CO}_3)_2$ ($n=48$). The FeCO_3 content is thus lower than that of rhombic

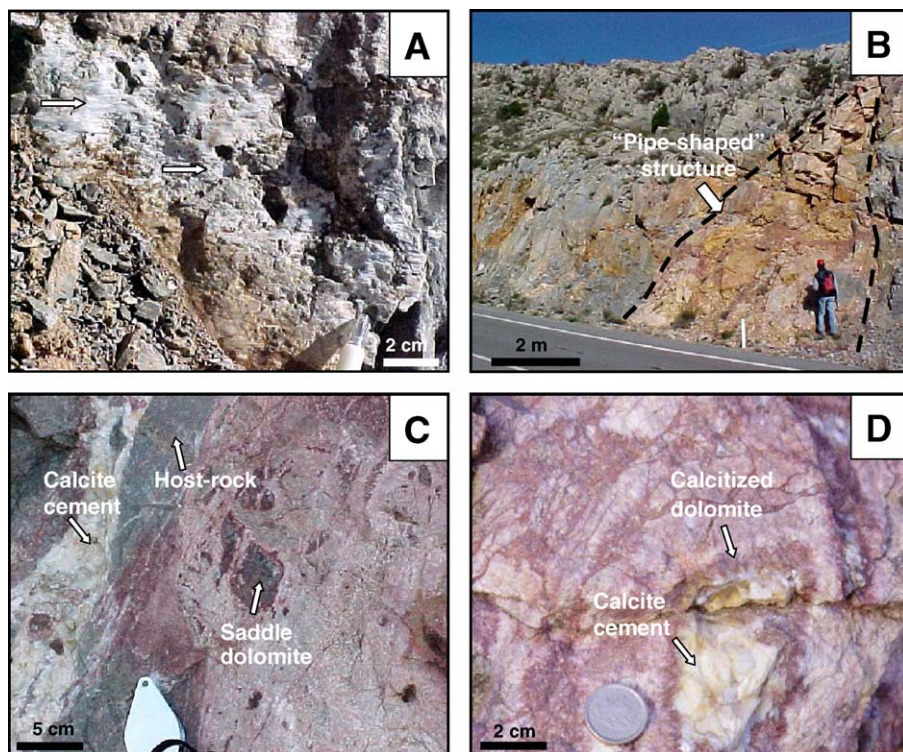


Fig. 5. Macroscopic view of the studied micro-structures. (A) Subvertical fault with dextral strike-slip component containing calcite mineral fibers with semi-horizontal striae (see arrows). (B) Chemical alteration and brecciation associated to NE-SW trending brittle fractures and faults. Note the “pipe-shaped” structure or “chimney”. (C) Detailed view of the previous picture showing limestone sample displaying fracture-fill calcite and *saddle* dolomite. (D) Another detailed view of the limestone showing big crystals of white calcite cement surrounded by red and breccified calcitized dolomite patches.

dolomite (3.6 % mol), as are the concentrations of Ba and Sr (Table 2). The $\delta^{18}\text{O}$ value of *saddle* dolomite in two samples are -11.5‰ and -11.3‰ and the $\delta^{13}\text{C}$ values $+2.1\text{‰}$ and $+2.2\text{‰}$ (Fig. 8).

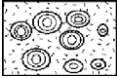

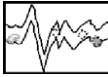


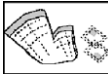

4.2.2.3. Calcitized dolomite. This calcite displays textural characteristics typical of *saddle* dolomite (Fig. 6-G), and a bright yellow luminescence with isolated, irregular, non-luminescent patches. The chemical composition is $(\text{Ca}_{0.991}\text{Mg}_{0.006}\text{Fe}_{0.003}\text{Mn}_0)\text{CO}_3$ ($n=12$). Sr values range from undetectable to 600 ppm, and Ba contents vary between undetectable and 734 ppm (Fig. 7). The $\delta^{18}\text{O}$ values of calcite range from -8.6‰ to -6.7‰ (with a single more negative value of -12.2‰) and $\delta^{13}\text{C}$ ratios range from -4.4‰ to $+0.2\text{‰}$ (Fig. 8).

4.2.2.4. Calcite cement. This cement occludes the central part of fractures, and hence post-dates rhom-

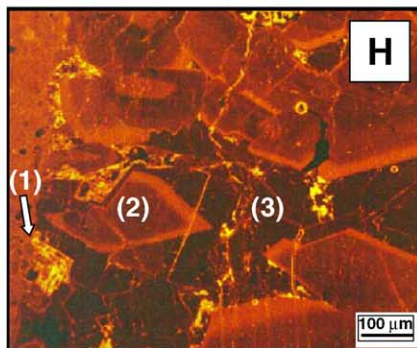
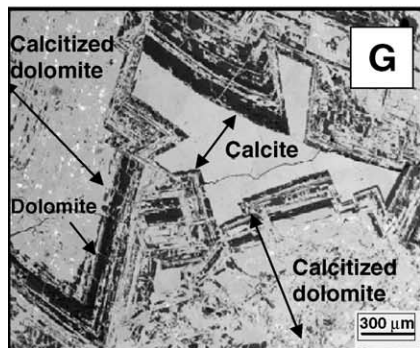
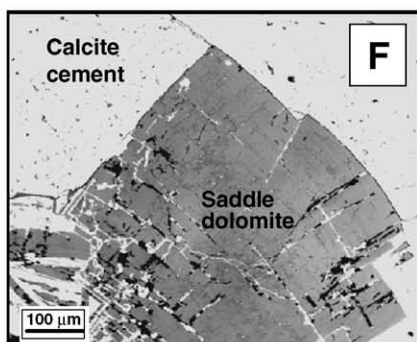
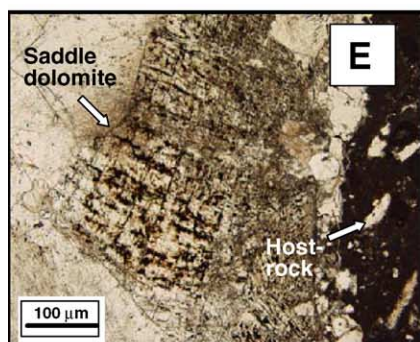
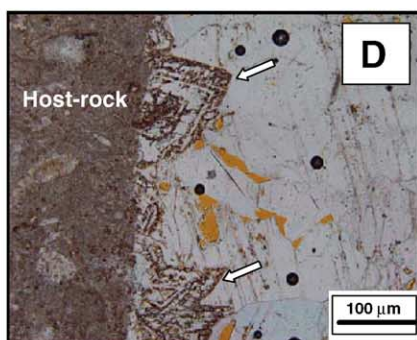
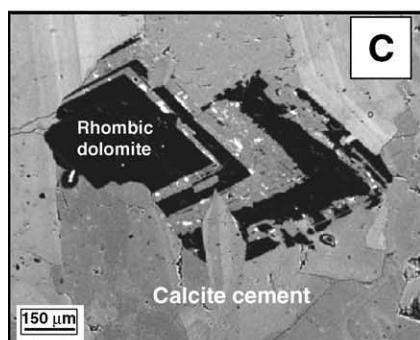
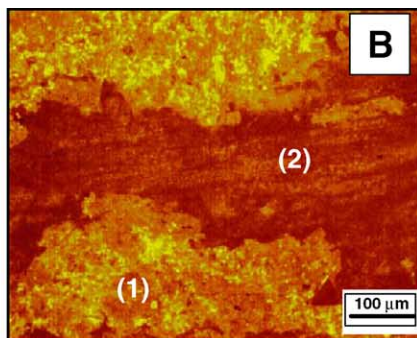
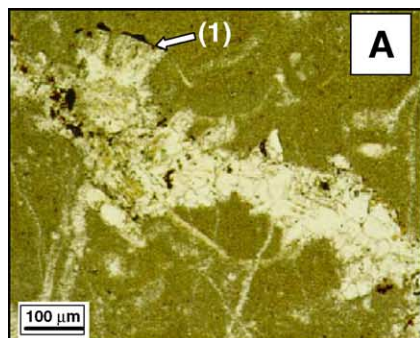
bic dolomite, *saddle* dolomite, and calcitized dolomite (Fig. 6-G). However, when this calcite cement is related to the “pipe-shaped” structure, extensive vuggy porosity remains, up to several centimeters in size (Fig. 9). The calcite shows widely varying crystal sizes with drusy (50 to 300 μm) and equant textures that form mosaics of large crystals (1.5 to 2.6 mm). Cathodoluminescence reveals dark-red to bright-red zoned crystals, post-dated by a non-luminescent fracture occluding cement (Fig. 6-H). The chemical composition of this calcite is $(\text{Ca}_{0.989}\text{Mg}_{0.009}\text{Fe}_{0.001}\text{Mn}_0)\text{CO}_3$ ($n=35$). The Sr content varies from undetectable to 1539 ppm and Ba ranges from undetectable to 1666 ppm (Fig. 7). This generation of calcite exhibits the highest values for both Sr and Ba. The $\delta^{18}\text{O}$ values are the most negative of all the carbonate phases examined (-13.4‰ to -10‰) and the $\delta^{13}\text{C}$ values are slightly positive ($+0.1\text{‰}$ to $+1.8\text{‰}$).

Table 1

Summary of the petrographic, cathodoluminescence, geochemical, fluid inclusion, and isotopic data for calcite and dolomite cements

Petrography	CL	Chemical composition	Th (°C)	Salinity (wt.% eq. NaCl)	$\delta^{18}\text{O}$ (VPDB)	$\delta^{13}\text{C}$ (VPDB)	$^{87}\text{Sr}/^{86}\text{Sr}^a$
<i>Host rock:</i>							
Calcite matrix and allochems 	Dark red matrix	$(\text{Ca}_{0.984}\text{Mg}_{0.013}\text{Fe}_{0.002}\text{Mn}_0)\text{CO}_3$ ($n=5$, matrix)	—	—	−7.2 to −4.9	+1.6 to +2.3	0.70723 to 0.70736
<i>First generation fractures (Ve1 and BPSe2):</i>							
Not cemented 	—	—	—	—	—	—	—
<i>Second generation fractures:</i>							
Cemented bed-parallel stylolites (g1).							
Calcite cement 	Outer zone: bright yellow calcite; inner zone: brownish orange calcite	$(\text{Ca}_{0.987}\text{Mg}_{0.011}\text{Fe}_{0.002}\text{Mn}_0)\text{CO}_3$ ($n=29$)	—	—	−8.8	+0.8	0.70775
Cemented vertical veins (g2) and “pipe- shaped” structure.							
Rhombic dolomite replacement cement 	Core: non-luminescent; outer zone: bright orange	$(\text{Ca}_{0.548}\text{Mg}_{0.415}\text{Fe}_{0.036}\text{Mn}_0)\text{CO}_3$ ($n=11$)	—	—	—	—	—
Saddle dolomite replacement cement 	Dull brown to non-luminescent curved crystal boundaries undulose extinction	$(\text{Ca}_{0.537}\text{Mg}_{0.448}\text{Fe}_{0.015}\text{Mn}_0)\text{CO}_3$ ($n=48$)	Primary FI: 110 to 155; mode=125	Primary FI: 21.5 to 23.5; mode=22.5	−11.5 to −11.3	+2.1 to +2.2	0.70796 to 0.70857
Calcitized dolomite 	Bright yellow calcite zones with scattered non-luminescent patches of dolomite	$(\text{Ca}_{0.991}\text{Mg}_{0.006}\text{Fe}_{0.003}\text{Mn}_0)\text{CO}_3$ ($n=12$)	—	—	−12.2 to −6.8	−4.4 to +0.2	0.70806 to 0.70845
Calcite cement 	Zoned dark-red to red euhedral calcite crystals predating non-luminescent pore filling/replacing calcite	$(\text{Ca}_{0.989}\text{Mg}_{0.009}\text{Fe}_{0.001}\text{Mn}_0)\text{CO}_3$ ($n=35$)	primary FI: 160 to 198; mode=170	Primary FI: 5.5 to 9.5; mode=7	−13.4 to −10	+0.1 to +1.8	0.70796 to 0.70801

^a Tithonian–Berriasian belemnites: 0.70715 to 0.70725 (Jenkyns et al., 2002).



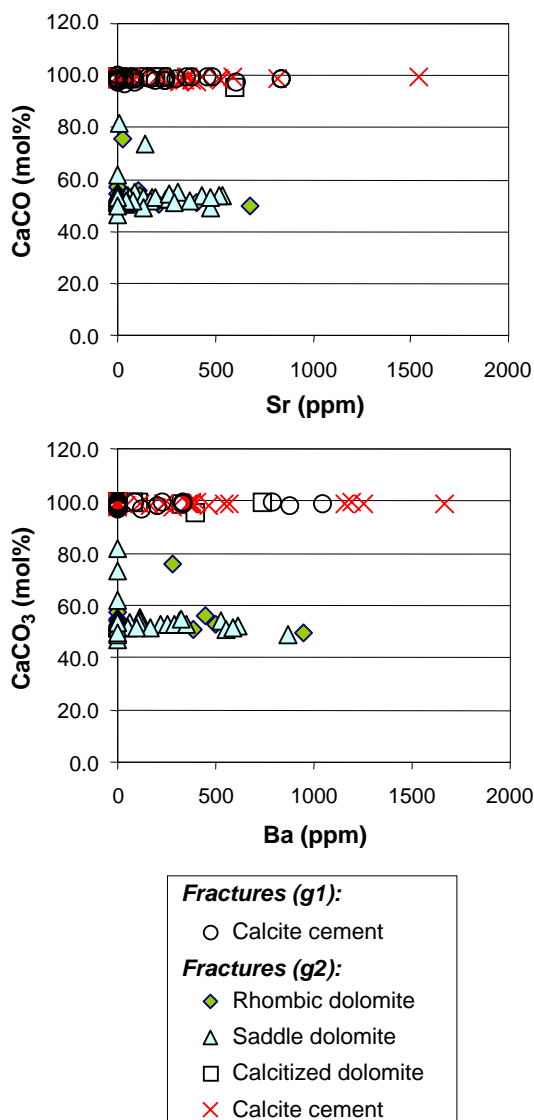


Fig. 7. Cross-plots of CaCO_3 vs. Sr and CaCO_3 vs. Ba in carbonate cements showing the relatively low Sr content in the saddle dolomite and calcite cements; and the presence of two different phases of calcite cements, poor and rich in Ba. Saddle and rhombic dolomite show variable abundance of Ba.

4.2.3. Sr isotopes

The $^{87}\text{Sr}/^{86}\text{Sr}$ ratios (Table 1, Fig. 10) of calcite host rock range from 0.70723 to 0.70736, which are slightly higher than Tithonian–Berriasian belemnites (0.70715 to 0.70725; Jenkyns et al., 2002). Only one ratio was obtained for calcite in cemented bed-parallel stylolites (0.70775), which is slightly higher than the host rock (0.70723 to 0.70736). The ratios in *saddle* dolomite range from 0.70796 to 0.70857. Calcitized dolomite ratios range from 0.70806 to 0.70845, which is, within the range of ratios of *saddle* dolomite. Ratios in calcite cement cluster around 0.70800. All cements are more radiogenic than the host rock or the belemnite standard (Table 1, Fig. 10).

4.2.4. Idiomorphic quartz and associated kaolin

Idiomorphic quartz crystals (~100 μm in size) with abundant calcite inclusions occur in association with both extensional fractures (g1) and (g2). In (g1), quartz is distributed at the peaks of the stylolites (Fig. 11-A). In the host rock, quartz crystals associated with inter-granular or micro-fracture porosity also occur. In (g2) fractures, idiomorphic quartz (0.5 to 2 mm in size) is much more abundant, and is surrounded by calcitized dolomite residue and Fe-oxide. A detrital clean core of quartz with micrite rim is overgrown with idiomorphic quartz (Fig. 11-B). Some idiomorphic quartz crystals enclose micritic patches or carbonate grains (Fig. 11-C). Pore-filling dickite (confirmed by X-ray analyses) occurs in (g2) fractures and is associated with the idiomorphic quartz, calcitized dolomite and Fe-oxide (Fig. 11-D). These phases are enclosed and isolated in the oncolitic limestone (Fig. 11-D), where it is difficult to establish textural relationship.

4.3. Fluid inclusions petrography and microthermometry

Large enough fluid inclusions (size > 15 μm) have been selected and measured in dolomite, calcite and

Fig. 6. Photomicrographs of authigenic carbonate minerals. (A) Optical micrograph (plane polarized) showing the boundary between the curved faces of the calcite crystals and the host rock (1). (B) Calcite cement with bright yellow luminescence in outer zone (1) and dull orange luminescence in inner zone (2) fills bed-parallel stylolites. (C) Backscattered electron image showing isolated rhombic dolomite, surrounded by calcite cement. (D) Optical micrograph (plane polarized light) illustrating rhombic dolomite in contact with the host rock (see arrows) (E) Thin band of *saddle* dolomite occurring on the margins of the subvertical extensional fractures (plane polarized). (F) Backscattered electron image showing *saddle* dolomite with characteristic curved faces. (G) Curved crystal faces highlighted by Fe-oxide of zoned calcitized dolomite cement (backscattered electron image). (H) Cathodoluminescence image of bright-yellow rhombic dolomite (1), dark-red to bright-red euhedral calcite zoned crystals (2), post-dated by non-luminescent fracture occluding calcite cement (3).

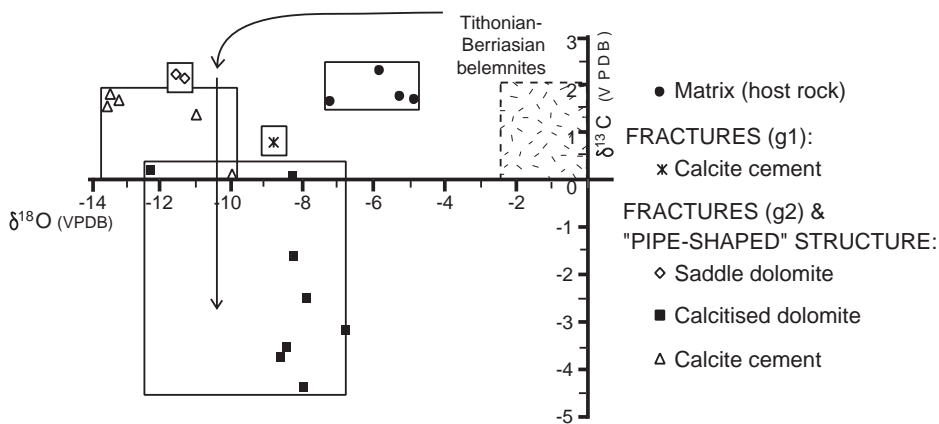


Fig. 8. Cross-plot of oxygen and carbon stable isotopic composition of calcite and dolomite phases showing the possible fluid evolution from the marine host rock limestones to saddle dolomite and calcite cement. Oxygen depletion of *saddle* dolomite and calcite cement suggests high precipitation temperature. The calcitized dolomite shows the typical meteoric pattern (Heydari, 1997). The range for Tithonian–Berriasian belemnites is from Jenkyns et al. (2002).

quartz cements. Notation of the fluid inclusion types follows the nomenclature of Boiron et al. (1992), which takes into account the nature of the dominant chemical phases and the type of phase change. The

relative chronology of the fluid inclusions is deduced from textural observations. On the basis of textural relationships and microthermometric measurements, two types of fluids have been distinguished associated

Table 2
Synthesis of the electron-microprobe analyses for calcite and dolomite

	(ppm)	Ca	Mg	Fe	Mn	Ba	Sr
<i>Matrix (host rock):</i>							
(n=5)	<i>Min.</i>	381389	1706	<n.d.	<n.d.	<n.d.	<n.d.
	<i>Max.</i>	398877	4287	4166	362	448	431
	<i>Average</i>	386526	3176	1223	148	125	306
<i>First generation fractures (cemented bed-parallel stylolites, g1):</i>							
<i>Calcite cement (n=29)</i>							
	<i>Min.</i>	381382	537	<n.d.	<n.d.	<n.d.	<n.d.
	<i>Max.</i>	411520	6982	5130	506	1048	837
	<i>Average</i>	395589	2698	995	107	139	213
<i>Second generation fractures (g2) and “pipe-shaped” structure:</i>							
<i>Rhombic dolomite (n=11)</i>							
	<i>Min.</i>	207197	49842	3902	<n.d.	<n.d.	<n.d.
	<i>Max.</i>	296319	120891	42525	731	949	676
	<i>Average</i>	225824	104332	20870	218	233	171
<i>Saddle dolomite (n=48)</i>							
	<i>Min.</i>	205889	45446	<n.d.	<n.d.	<n.d.	<n.d.
	<i>Max.</i>	340980	126089	76026	912	869	541
	<i>Average</i>	225479	114359	9132	194	126	125
<i>Calcitized dolomite (n=12)</i>							
	<i>Min.</i>	385491	289	<n.d.	0	<n.d.	<n.d.
	<i>Max.</i>	406317	3178	19385	340	734	600
	<i>Average</i>	395543	1351	1798	94	137	113
<i>Calcite cement (n=35)</i>							
	<i>Min.</i>	386335	663	<n.d.	<n.d.	<n.d.	<n.d.
	<i>Max.</i>	412207	5312	2169	506	1666	1539
	<i>Average</i>	396783	2255	809	100	280	222

Data reported as minimum, maximum and average values.
<n.d.=less than the reporting limit; n=number of analyses.

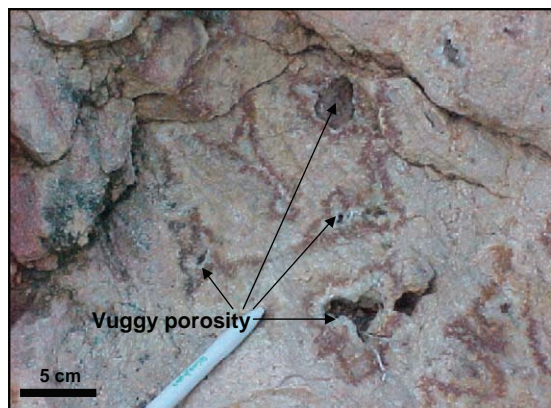


Fig. 9. Photograph showing dissolution-enlarged vuggy porosity, up to several centimetres in size. This porosity is partially occluded by calcite cement in the “pipe-shaped” structure or “chimney”.

with fracture-filling carbonate cements and authigenic quartz (Table 3). The first fluid type is characterised by moderate temperature (Fig. 12) and high salinity, and has been recognised in *saddle* dolomite crystals, in non-luminescent fracture occluding calcite cement (Fig. 6-H) and in idiomorphic quartz crystals. The second fluid type has moderate to high temperature and moderate salinity, and has only been recognised in dark-red to bright-red zoned calcite cement (Fig. 6-H).

They are all aqueous and no C–N–S species were detected.

Primary subidiomorphic fluid inclusions (liquid + vapour) along growth planes in *saddle* dolomite have T_m ice values indicating a high salinity fluid (21.5 to 23.5 wt.% eq. NaCl, mode 22.5 wt.% eq. NaCl) and homogenisation temperatures ranging between 110–155 °C (mode 125 °C).

Idiomorphic primary inclusions (liquid + vapour) occur along growth planes in the last non-luminescent phase of the calcite crystals. Although the first melting of ice is not clearly observable and not reflected in Table 3, it takes place around –25 °C in host mineral. Even though this eutectic temperature could be attributed to a recrystallisation of the solid phase, the eutectic melting behaviour of the H₂O–NaCl system has been defined between a metastable eutectic at –28 °C and the stable eutectic temperature at –21.2 °C (Goldstein, 2001). Therefore, a eutectic melting around –25 °C is consistent with the interpretation of an aqueous solution belonging to this system. The T_m ice values (–10.5 to –3.5 °C; mode –6 °C) indicate moderate salinity (5.5 to 9.5 wt.% eq. NaCl; mode 7 wt.% eq. NaCl). Homogenisation temperatures range between 160 and 198 °C (mode 170 °C) (Fig. 12). A second

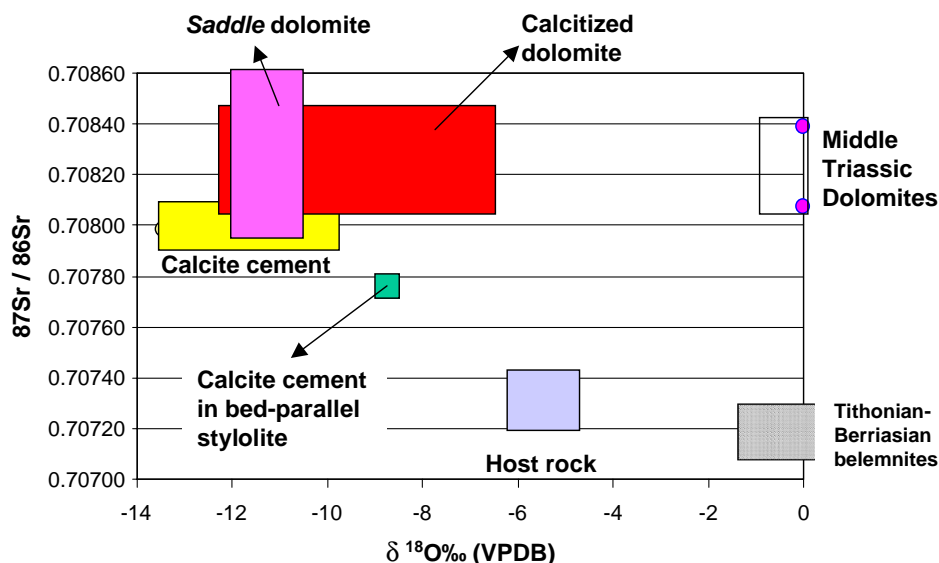


Fig. 10. Cross plot of $^{87}\text{Sr}/^{86}\text{Sr}$ ratios versus $\delta^{18}\text{O}$ (VPDB) showing that all cements are more radiogenic than the host rock or the Tithonian–Berriasian belemnites (Jenkyns et al., 2002). The range for Middle Triassic dolomites is also represented (after Calvet et al., 2001).

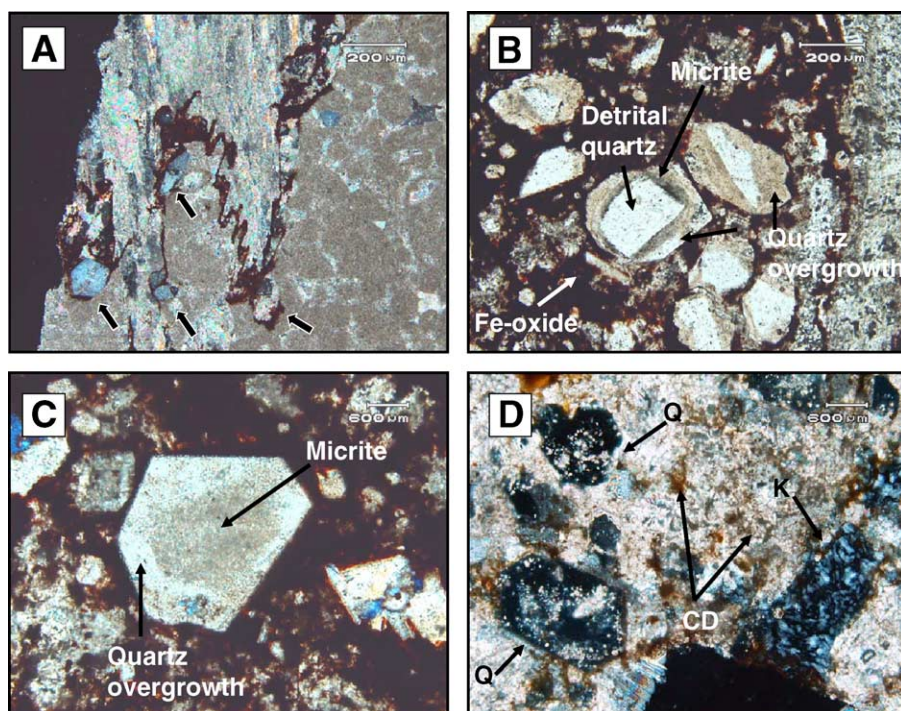


Fig. 11. Optical micrographs of idiomorphic quartz. (A) Note the close growth of the quartz crystals at the peaks of the stylolites (see arrows); polarized light. (B) Detrital quartz grains with micrite rims that are overgrown with idiomorphic quartz (plane light). (C) Idiomorphic quartz crystals enclosing micritic patches or grains (plane light). (D) Dickite pore-fill (k) associated with idiomorphic quartz (Q) and calcitized dolomite (CD; polarized light).

type of subidiomorphic fluid inclusions (liquid+vapour) trapped later than those described above has been classified as secondary trails of fluid inclusions in calcite crystals. There are not enough textural data to argue a primary origin, but it cannot be ruled out. The T_m ice values correspond to a high salinity fluid, ranging between 15 and 19.7 wt.% eq.NaCl, with a modal value of 19.1 wt.% eq.NaCl. The homogeni-

sation temperatures range between 110–125 °C (mode 110 °C).

Primary subidiomorphic fluid inclusions (liquid+vapour) along growth planes at the quartz cement reveal that the salinity values are 13.1 to 15.5 wt.% eq.NaCl (mode 13.6 wt.% eq.NaCl) and the homogenisation temperatures range between 140 and 180 °C (mode 178 °C) in idiomorphic quartz (Fig. 12).

Table 3
Summary of fluid inclusions petrography and microthermometry

Host mineral	Calcite cement		Saddle dolomite	Idiomorphic quartz overgrowth
Composition	H ₂ O–NaCl	H ₂ O–NaCl–(CaCl ₂)	H ₂ O–NaCl–(CaCl ₂)	H ₂ O–NaCl–(CaCl ₂)
Petrography	Primary	Secondary	Primary	Primary
Habit (room T)	Biphasic	Biphasic	Biphasic	Biphasic
% vapor phase	10–20	5–15	5–15	10–15
T_c (°C)	–	<–40	<–40	<–35
T_m ice (°C)	–10.5/–3.5 mode: –6	–16/–11 mode: –15.5	–21.5/–19 mode: –20	–11.5/–9.2 mode: –9.7
T_h (°C)	160/198 mode: 170 (L)	100/125 mode: 110 (L)	110/155 mode: 125 (L)	140/180 mode: 178
Salinity (wt.% eq. NaCl)	5.5/9.5 mode: 7	15/19.7 mode: 19.1	21.5/23.5 mode: 22.5	13.1/15.5 mode: 13.6
Density (gr/cm ³)	0.8/1 mode: 0.9	1/1.1 mode: 1	1/1.1 mode: 1	0.9/1 mode: 1

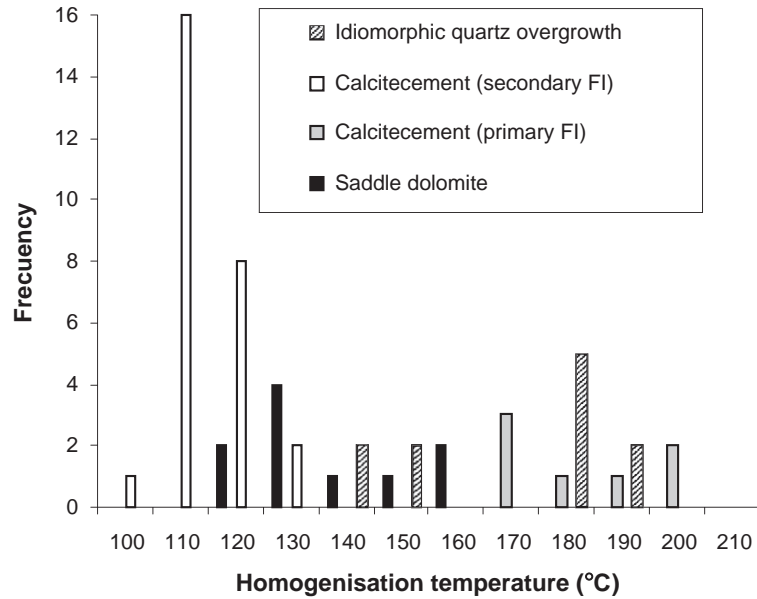


Fig. 12. Histogram of homogenisation temperatures in primary and secondary fluid inclusions in saddle dolomite, calcite and quartz. Notice the presence of two populations of fluid inclusion homogenisation temperatures in the calcite phases.

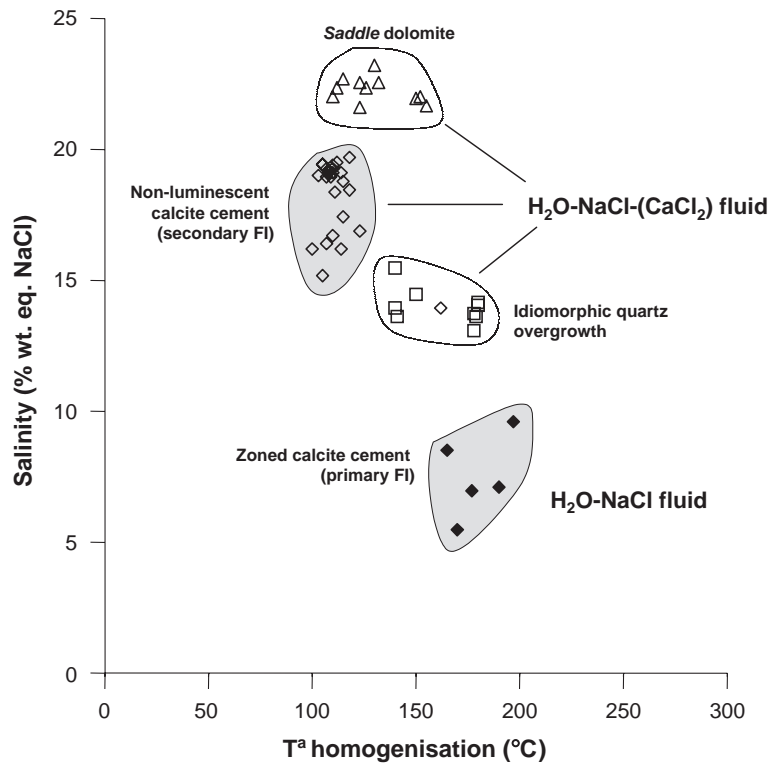


Fig. 13. Cross-plot of salinity versus homogenisation temperature for fluid inclusions in saddle dolomite, in the two calcite phases and in the authigenic idiomorphic quartz. Note that the two calcite phases are plotted separately in this diagram.

Values of $T_c < -40$ °C of secondary fluid inclusions in calcite cement and primary fluid inclusions in *saddle* dolomite and quartz cement are lower than the H_2O –NaCl system eutectic temperature (-21.5 °C). It could be explained by a metastable eutectic involving phases like hydrohalite, that is a process described in several systems (Davis et al., 1990), or by the presence of salts like $CaCl_2$ in the fluid inclusions that decrease the first melting temperature (Shepherd et al., 1985). In addition to the final melting of ice, the final melting of hydrohalite is a characteristic feature of the system H_2O –NaCl– $CaCl_2$ (Zwart and Tourent, 1994; Martín-Crespo et al., 2002). The last melting of hydrohalite ($NaCl \cdot 2H_2O$) was not observed, and the anomalously low eutectic temperature can be attributed to the presence of others salts like $CaCl_2$ in the fluid that decrease the eutectic temperature. Although these inclusions show a low eutectic temperature, they do not show others characteristics features of the H_2O –NaCl– $CaCl_2$ system like a typical brown colour and melting of hydrohalite (Zwart and Tourent, 1994), and seems to be controlled by the H_2O –NaCl system and not by H_2O –NaCl– $CaCl_2$.

Homogenisation temperature vs. salinity plot displays four clusters (Fig. 13). Although fluid inclusions belonging to the system H_2O –NaCl–($CaCl_2$) show slight differences in temperature and salinity in each mineral (*saddle* dolomite, non-luminescent calcite and authigenic quartz), all of them have the same textural features and microthermometric behaviour, and have been defined by the same fluid inclusions type. The cluster defined by the H_2O –NaCl system in zoned calcite shows different textural and microthermometric features (lower density, higher % vapour phase, lower salinity), and can be characterised by a different fluid.

5. Discussion

Two important issues need to be addressed in order to understand the origin and significance of the dolomite–calcite cemented fractures and the formation of the quartz in the Bovalar Formation, including: 1) the timing of fracturing relative to cementation in the context of the structural history of the Alpine deformation, and 2) the origin and geochemical evolution of the fluids.

The carbonate-cemented fractures have been developed during the Alpine deformation (Álvaro et al., 1979; Simón, 1986; Capote et al., 2002). These structures occur as stylolites, extensional fractures and the “pipe-shape” fault related structure in the Early Tithonian–Berriasian limestones. Field observations, cross-cutting relationships and previous studies on stress analysis, and ages of related deposits (Simón, 1986; Liesa, 2000) suggest formation during the post-rift Alpine deformation. Thus, the fractures are treated as part of a regional deformation and are considered to be formed during the Late Eocene–Miocene compressional and Miocene–Pliocene extensional phase (Simón, 1984, 1986; Liesa, 2000; Salas et al., 2001). The overall pattern of fracturing and associate cementation of the area is summarized in Table 4.

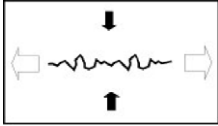

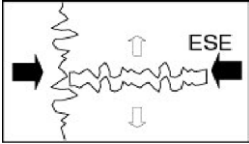
Regional deformation was accompanied by several dolomite and calcite cementation events. The first generation of fractures (g1) developed due to an ESE–WNW compression (late Eocene–Miocene) stress field (Table 4), and was initially cemented by *saddle* dolomite. Only relicts of this dolomite phase remain, as it has been almost completely calcitized. Calcitization was followed by calcite cementation, occluding the central part of these fractures. Stable and radiogenic isotopes (Table 1) likely reflect a mixture of these carbonate phases, thus the composition of the fluids involved in this calcite precipitation cannot be readily deduced.

Four phases of carbonate cement occluded the second generation (g2) subvertical extensional fractures and the “pipe-shape” fault-related structures, which were developed during the late post-rift (Miocene–Pliocene) extensional Alpine tectonic regime of the Iberian Range (Simón, 1984, 1986).

Saddle dolomite, which occurs not only as cement in fractures, but also as a replacement of host rock adjacent to the “pipe-shape” structure and the breccia is a typical feature of “chimneys” structures formed by high-pressured hydraulic fracturing (cfr. Sibson, 1994; Aranburu et al., 2002). Fluid inclusions in the dolomite have mean homogenisation temperature of 125 °C, low $\delta^{18}O$ values and $^{87}Sr/^{86}Sr$ ratios that are more radiogenic than the host rock (Table 1). The maximum temperature reached in the Bovalar Formation was 110 °C (confirmed by vitrinite reflectance and fluid inclusions), as has been reported by Permanyer et al. (2001) for the site of greatest subsidence in the Maes-

Table 4

Alpine deformation stages and their relation to fracture fill cements and hypothetical fluids

	Pre-Alpine	Alpine deformation					
Geodynamic regime		Compressional stage		Extensional stage			
Age	<i>Mesozoic</i>	Late Eocene–Miocene		Miocene–Pliocene			
Strike	–	NE (070°)		NNE–NE and ESE			
Type of fracture	Bed-parallel stylolites	a) Vertical stylolites (Ve1) & faults		c) Second generation fractures (g2) and “pipe-shaped” fault related structure			
							
Cements	–	–	<i>Saddle</i> dolomite dedolomite & calcite	<i>Saddle</i> dolomite	Dedolomite	Calcite	Quartz overgrowth
Fluids	–	–	?	Hydrothermal	Meteoric	Hydrothermal	Hydrothermal
Temperature (mode)	–	–	–	125 °C	–	110 to 170 °C	178 °C
Salinity	–	–	–	high	–	high to low	low

trat Basin. Consequently, *saddle* dolomite can be considered as a “hydrothermal” product formed at a higher, >5–10 °C, than ambient temperature (Machel and Lonnee, 2002). Moreover, the fact that *saddle* dolomite is enriched in ^{87}Sr relative to the marine ratios is consistent with a significant source of radiogenic siliciclastic-derived allochthonous fluids into permeable carbonates during burial. Most studies invoke a model whereby *saddle* dolomite precipitated from highly evolved basinal brines during deep burial (Spötl and Pitman, 1998).

The homogenisation temperatures and the high salinity values of the fluid inclusions, suggest that the fluid involved in *saddle* dolomite precipitation is consistent with a saline, Sr-enriched hydrothermal fluid that migrated upwards along fractures and faults under elevated pressures, suggested by the breccified and the external morphology of the “pipe-shape” structure. This fluid flow probably occurred during the Miocene extensional stage of tectonism. The elevated pressure could have been generated in several ways, but all are closely associated with faulting (e.g., Knipe, 1993; Sibson, 1994). Mg ions in the fluids could have been sourced from fluid interaction with magnesium rich mudrocks from the underlying Late Triassic (Marfil, 1970) or volcanics (Searl and Fallick, 1990; Morad et al., 1996). The Lower and Middle Jurassic alkaline volcanic rocks outcropping in this area of the Iberian Range (Aurell et al., 2002) could be the source of the heated saline fluids.

Following the formation of *saddle* dolomite, the calcitized dolomite is characterised by $\delta^{13}\text{C}$ ratios ranging from -4.4‰ to $+0.2\text{‰}$ (Fig. 8), which reflect contribution of soil-derived CO_2 during exposure to meteoric fluids (Lohmann, 1987; Heydari, 1997; Al-Aasm, 2000). This calcite is related to meteoric water infiltrated through fractures and probably took place during the extensional stage of Alpine deformation (Table 4).

The last carbonate phase to precipitate was calcite cement occluding (g2) fractures and rimming the vuggy pores in the “pipe-shaped” structure. This cement has low $\delta^{18}\text{O}$ ratios and $^{87}\text{Sr}/^{86}\text{Sr}$ ratios which are more radiogenic than the host rock and slightly lower than the *saddle* dolomite (Fig. 10). A cross-plot of homogenisation temperatures versus salinity (Fig. 13) shows two groups of data reflecting the presence

of two different phases of calcite as were observed under cathodoluminescence (Fig. 6-H). Based on the high homogenisation temperature data, both of these calcite cements can be considered as hydrothermal in origin (Machel and Lonnee, 2002). Hence, the fluid involved in the precipitation of these late calcite cements initially had moderate salinity and high temperature and must have evolved to a lower temperature and higher salinity fluid (both Sr enriched; cfr. Sellwood et al., 1989). These fluids were probably derived from the mixing of saline fluids with descending meteoric water that migrated via fractures during extensional Miocene–Pliocene Alpine stage deformation (Table 4).

The development of vuggy porosity can be related to the circulation of these fluids, which is a characteristic feature of hydrothermal and dissolution cavities (Aranburu et al., 2002). Carbonate precipitation and dissolution occur within hydrothermal cavities due to several conditions such as elevated temperature gradients, changes of pressure and temperature of upwelling fluids, elevated rate of discharge and mixing of waters of contrasting chemistry (Dublyansky, 2000). Additionally the limestones in the Casablanca oil field (Late Kimmeridgian–Portlandian) in the Mediterranean Sea are affected by processes of brecciation, corrosion vugs, dolomite and calcite cements, which have been interpreted as hydrothermal karst processes (Vallaure et al., 2003). These authors reported that the final sequence of events include the formation of kaolinite, dolomite, quartz cement and oil stain. The morphology, textural and geochemical data of the “pipe-shaped” structure, show close similarities to the hydrothermal karst described by Vallaure et al. (2003) in the limestones of the Casablanca oil field.

Fracture-filling carbonate cements (*saddle* dolomite, calcitized dolomite and calcite cement) show a wide range of $^{87}\text{Sr}/^{86}\text{Sr}$ ratios (Table 1 and Fig. 10), which are comparable with the $^{87}\text{Sr}/^{86}\text{Sr}$ ratios reported by Calvet et al. (2001) for the Middle Triassic dolomites and evaporites in the Iberian Range, and with the ore-stage calcite from the Aptian limestone in the Maestrat Basin (Grandia et al., 2003). The, higher values (0.71088 to 0.71800) for the carbonate filled the fractures during the Lower and Middle Miocene (Travé and Calvet, 2001), thus ruling out Miocene seawater as a fluid source. Therefore, Sr enrichment of

the studied carbonate cements suggests a deep origin and circulation of the fluids involved in the carbonate cement precipitation, rather than fluids originating from Miocene seawater.

Fluid inclusions in authigenic quartz have higher homogenisation temperatures but lower salinities than inclusions in the *saddle* dolomite (Figs. 12 and 13 and Table 3). In modern hydrothermal systems, mineralisation is localised to fractures, vugs and breccias with associated minerals such as quartz, pyrite and chalcopyrite as well as calcite and dolomite (Counter and Lowenstein, 1997). Likewise, Spötl and Pitman (1998) suggest that saline pore-waters involved in *saddle* dolomite precipitation are commonly close to equilibrium with a number of minerals including fluorite, pyrite, sphalerite and quartz. In addition, dickite formation has been described as indicator of regional thermal events (Keller, 1988) and in tectonic environment precipitating directly in fractures, contemporaneously with calcite veinlets (Buatier et al., 1997). Thus the high temperature of the authigenic quartz and its association with dickite could also point out to precipitation from a hydrothermal fluid.

6. Conclusions

The results of this study allow us to characterise hydrothermal fluid circulation events in the Maestrat Basin, Eastern Iberian Range. These events were structurally controlled and occurred during the extensional phase of the Alpine Orogeny (Miocene–Pliocene). Three principal fractures filled by carbonate cements were recognised, including cemented bed-parallel stylolites and the first generation fractures, the second generation subvertical extensional fractures and the “pipe-shaped” fault related structure.

First generation fractures were cemented during the Late Eocene–Miocene compressional stage by *saddle* dolomite, which was later almost completely calcitized, and calcite cement. Second generation subvertical extensional fractures and “pipe-shaped” fault-related structure were cemented by four generations of carbonate cement during the Miocene–Pliocene extensional stage of the Alpine Orogeny: (i) the first carbonate phase is rhombic dolomite, which precipi-

tated locally, (ii) the fluid involved in the fracture fill by *saddle* dolomite was characterised by high salinity and temperature, hydrothermal, dolomitising and radiogenic Sr-enriched. This origin is supported by the salinity results of the FI and by the $^{87}\text{Sr}/^{86}\text{Sr}$ ratios similar to the Triassic dolomites and evaporites. The magnesium source for dolomite precipitation could be related to the Mg-rich mudrocks and evaporites of the underlying Late Triassic, (iii) *saddle* dolomite cement and replacement was followed by an input of meteoric water, which was confirmed by the isotopic data and related to the extensional stage of tectonism, (iv) finally, late calcite cement precipitated from fluids with increasing in salinity and decreasing in temperature. These fluids are interpreted as hydrothermal and radiogenic Sr-enriched based on T_h data and high $^{87}\text{Sr}/^{86}\text{Sr}$ ratios. Fractures were occluded by the late calcite cement, but major vuggy porosity remains in the “pipe-shaped” structure, which is probably related to a hydrothermal karst. The high temperatures and salinities are also registered by the fluid inclusions in authigenic quartz and the presence of dickite indicating that these phases also precipitated from hydrothermal fluids in a later stage.

This work contributes to understand the timing, the origin and the evolution of fluids responsible for the dolomitisation and hydrothermal events, which is essential for the evaluation of the economic potential of the Iberian Range and adjacent offshore basins of the Mediterranean Sea.

Acknowledgments

Funding was provided by the research project DGI-CYT BTE2000-0574-C03-02 and 01-LEC-EMA10F (REN2002-11404-E) of the European Science Foundation to Rafaela Marfil, *Natural Sciences and Engineering Research Council of Canada* (NSERC) to Ihsan. S. Al-Aasm and by a post-doctoral contract “Juan de la Cierva” (MCyT) to Miguel A. Caja. Special thanks go to R.A.J. Swennen, R. Capote, A. Travé, M. Cioppa and M.I. Benito for their comments and help. Many thanks to the two anonymous reviewers and the editor who helped to improve and focus this paper. Also thanks to Fernández-Larios for his assistance with the electron microprobe.

References

- Al-Aasm, I.S., 2000. Chemical and isotopic constraints for recrystallization of sedimentary dolomites from the Western Canada Sedimentary Basin. *Aquatic Geochemistry* 6, 227–248.
- Al-Aasm, I.S., Taylor, B.E., South, B., 1990. Stable isotope analysis of multiple carbonate samples using selective acid extraction. *Chemical Geology* 80, 119–125.
- Albert, J.F., 1976. Estudio geotérmico preliminar de Cataluña. PhD Thesis, Universidad de Barcelona, 460 pp.
- Álvaro, M., Capote, R., Vegas, R., 1979. Un modelo de evolución geotectónica para la Cadena Celtibérica. *Acta Geologica Hispanica Homenaje a L. Solé Sabarrís* 14, 172–177.
- Aranburu, A., Fernández-Mendiola, P.A., López-Horgue, M.A., Gracia-Mondejar, J., 2002. Syntectonic hydrothermal calcite in a faulted carbonate platform margin (Albian of Jorrios, northern Spain). *Sedimentology* 49, 875–890.
- Aurell, M., Mas, R., Meléndez, A., Salas, R., 1994. El tránsito Jurásico–Cretácico en la Cordillera Ibérica: relación tectónica–sedimentación y evolución paleogeográfica. *Cuadernos Geología Ibérica* 18, 369–396.
- Aurell, M., Meléndez, G., Olóriz, F., Bádenas, B., Caracuel, J.E., García-Ramos, J.C., Goy, A., Linares, A., Quesada, S., Robles, S., Rodríguez-Tovar, F.J., Rosales, I., Sandoval, J., Suárez de Centi, C., Tavera, J.M., Valenzuela, M., 2002. Jurassic. In: Gibbons, W., Moreno, T. (Eds.), *The Geology of Spain*. The Geological Society, pp. 212–253.
- Black, D.F.B., Mac Quown, W.C., Dettaas, R.J., 1981. The relation of dolomite associated with faults to the stratigraphy and structure of Central Kentucky. *Contributions to the Geology of Kentucky*, Geological Survey of Professional Paper, vol. 1151-A, pp. A1–A19.
- Boiron, M.C., Essarraj, S., Sellier, E., Cathelineau, M., Lespinasse, M., Poty, B., 1992. Identification of fluid inclusions in relation to their host microstructural domains in quartz by cathodoluminescence. *Geochimica et Cosmochimica Acta* 56, 175–185.
- Buatier, M., Travé, A., Labaume, P., Potdevin, J.P., 1997. Dickite related to fluid–sediment interaction and deformation in Pyrenean thrust-fault zones. *European Journal of Mineralogy* 9, 875–888.
- Calvet, F., López-Gómez, J., Galindo, C., Tucker, M.E., Arche, A., 2001. Dolomías de gran escala en las plataformas epeiricas triásicas del este de la Península Ibérica. *Geotemas* 3 (1), 105–107.
- Canals, A., Cardellach, E., 1996. Caracterización de los fluidos en sucesivas fases de fracturación de las Cadenas Costero Catalanas y su registro en los filones de Ba–F de baja temperatura. *Geogaceta* 20, 696–699.
- Capote, R., Muñoz, J.A., Simón, J.L., Liesa, C.L., Arlegui, L.E., 2002. Alpine tectonics I: the Alpine system north of the Betic Cordillera. In: Gibbons, W., Moreno, T. (Eds.), *The Geology of Spain*. The Geological Society, pp. 367–400.
- Counter, K., Lowenstein, T.K., 1997. Carbonate-hosted mineralization of the Lower Ordovician Ogdensburg Formation: evidence for a Paleozoic anomaly in the St. Lawrence–Ottawa lowlands of New York and Ontario. In: Montañez, I.P., Gregg, J.M., Shelton, K.L. (Eds.), *Basin-Wide Diagenetic Patterns: Integrated Petrologic, Geochemical and Hydrologic Considerations*, SEPM Special Publication, vol. 57, pp. 207–218.
- Davis, D.W., Lowenstein, T.K., Spencer, R.J., 1990. Melting behaviour of fluid inclusions in laboratory-grown halite crystals in the systems NaCl–H₂O, NaCl–KCl–H₂O, NaCl–MgCl₂–H₂O, and NaCl–CaCl₂–H₂O. *Geochimica et Cosmochimica Acta* 54, 591–601.
- Dublyansky, Y.V., 2000. Hydrothermal speleogenesis; its settings and peculiar features. In: Klimchouk, A., Ford, D., Palmer, A., Dreybrodt, W. (Eds.), *Speleogenesis evolution of karst aquifers*. National Speleological Society, Huntsville, AL, United States, pp. 292–297.
- Garreau, B., Charpal de, O.L., Montadert, L., Gubler, G., Rouge, P.E., Baron, G.A., Favre, J.H., 1959. Contribution française a l'étude de la dolomitisation. Report intern de l'Institut Française du Pétrole, Section I-Paper 3, 53–80.
- Goldstein, R.H., 2001. Fluid inclusions in sedimentary and diagenetic systems. *Lithos* 55, 159–193.
- Grandia, F., Asmerom, Y., Getty, S., Cardellach, E., Canals, A., 2000. U–Pb dating of MVT ore-stage calcite: implications for fluid flow in a Mesozoic extensional basin from Iberian Peninsula. *Journal of Geochemical Exploration* 69–70, 377–380.
- Grandia, F., Cardellach, E., Canals, A., 1999. Fluid mixing evidence in MVT Zn–Pb deposits related to rift stage carbonates of the Maestrat Basin, Eastern Spain. In: Stanley, F., et al., (Eds.), *Mineral Deposits: Processes to Processing*, pp. 861–864.
- Grandia, F., Cardellach, E., Canals, A., Banks, D.A., 2003. Geochemistry of the fluids related to epigenetic carbonate-hosted Zn–Pb deposits in the Maestrat Basin, Eastern Spain: fluid inclusion and isotope (Cl, C, O, S, Sr) evidence. *Economic Geology* 98, 933–954.
- Harris, J.F., 1991. The enigma of tectonic dolomitization and fracturing in Alibuckle exploration. *Oklahoma Geological Survey Circular* 92, 122–126.
- Heydari, E., 1997. Hydrotectonic models of burial diagenesis in platform carbonates based on formation water geochemistry in North American sedimentary basins. In: Montañez, I.P., Gregg, J.M., Shelton, K.L. (Eds.), *Basin-Wide Diagenetic Patterns: Integrated Petrologic, Geochemical and Hydrologic Considerations*, SEPM Special Publication, vol 57, pp. 53–79.
- Hurley, N.F., Budros, R., 1990. Albion–Scipio and Stoney Point fields — USA, Michigan Basin. In: Beaumont, I.E.A., Foster, N.H. (Eds.), *Stratigraphic Traps*. American Association of Petroleum Geologists, Tulsa, OK, pp. 1–37.
- Jenkyns, H.C., Jones, C.E., Gröcke, R., Hesselbo, S., Parkinson, D.N., 2002. Chemostratigraphy of the Jurassic System: applications, limitations and implications for palaeoceanography. *Journal of the Geological Society London* 159, 351–378.
- Jones, R.M.P., 1980. Basinal isostatic adjustment faults and their petroleum significance. *Bulletin of Canadian Petroleum Geology* 28, 211–251.
- Keller, W.D., 1988. Authigenic kaolinite and dickite associated with metal sulfides, probable indicators of a regional thermal event. *Clays Clay Minerals* 36, 152–158.
- Knipe, R.J., 1993. The influence of fault zone processes and diagenesis on fluid flow. In: Horbury, A.D., Robinson, A.G. (Eds.),

- Diagenesis and Basin Development, AAPG Studies in Geology, vol. 36, pp. 135–151.
- Liesa, C.L., 2000. Fracturación y campos de esfuerzos compresivos alpinos en la Cordillera Ibérica y el NE peninsular. PhD Thesis, Universidad de Zaragoza, p. 765.
- Lindholm, R.C., Finkelman, R.B., 1972. Calcite staining: semiquantitative determination of ferrous iron. *Journal of Sedimentary Petrology* 44, 428–440.
- Lohmann, K.C., 1987. Geochemical patterns of meteoric diagenetic systems and their applications to studies of paleokarst. In: James, N.P., Choquette, P.W. (Eds.), *Paleokarst*. Springer Verlag, New York, pp. 58–80.
- Machel, H.G., Anderson, J.H., 1989. Pervasive subsurface dolomitization of the Nisku Formation in Central Alberta. *Journal of Sedimentary Petrology* 59, 891–911.
- Machel, H.G., Lonnee, J., 2002. Hydrothermal dolomite a product of poor definition and imagination. *Sedimentary Geology* 152, 163–171.
- Machel, H.G., Mountjoy, E.W., 1986. Chemistry and environments of dolomitization—a reappraisal. *Earth-Science Review* 23, 175–222.
- Machel, H.G., Mountjoy, E.W., 1987. Pervasive dolomitization of the Devonian carbonates of Western Canada. *Bulletin of Canadian Petroleum Geology* 35, 143–158.
- Malone, M.J., Baker, P.A., Burns, S.J., 1996. Hydrothermal dolomitization and recrystallization of dolomite breccias from the Miocene Monterey Formation, Tepusquet Area, California. *Journal of Sedimentary Research* 66, 976–990.
- Marfil, R., 1970. Estudio petrogenético del Keuper en el sector meridional de la Cordillera Ibérica. *Estudios Geológicos* 26, 113–161.
- Martín-Crespo, T., Delgado, A., Vindel, E., López, J.A., Fabre, C., 2002. The latest Post-Variscan fluids in the Spanish Central System: evidence from fluid inclusion and stable isotope data. *Marine and Petroleum Geology* 19, 323–337.
- Morad, S., De Ros, L.F., Al-Aasm, I.S., 1996. Origin of low $\delta^{18}\text{O}$, pre-compactional ferroan carbonates in the marine Sto. Formation (Middle Jurassic), offshore NW Norway. *Marine and Petroleum Geology* 13, 263–276.
- Nadal, J., 2000. Dolomías relacionadas con fallas durante la etapa de rift Jurásico superior–Cretácico inferior en la subcuenca de la Salzedella (Cuenca del Maestrazgo, Cadena Ibérica). *Geotemas* 1 (2), 247–252.
- Nadal, J., 2001. Estudi de la dolomitació del Juràssic superior–Cretaci inferior de la cadena ibèrica oriental i la cadena costanera catalana: Relació amb la segona etapa de rift mesozoica. PhD Thesis, Universidad de Barcelona. 443 pp.
- Packard, J.J., Pellegrin, G.J., Al-Aasm, I.S., Samson, I., Gagnon, J., 1990. Diagenesis and dolomitization associated with hydrothermal karst in Famennian Upper Wabamun ramp sediments, northwestern Alberta. In: Bloy, G.R., Hadley, M.G. (Eds.), *The Development of Porosity in Carbonate Reservoirs*, C.S.P.G. Continuing Education Short Course Notes, vol. 9, pp. 1–19.
- Permayer, A., Salas, R., Rossi, C., 2001. Contribution of organic geochemistry to integrated studies on sedimentary basin evolution. In: Lago, M., Arranz, E., Galé, C. (Eds.), III Congreso Ibérico de Geoquímica, VIII Congreso de Geoquímica de España, Zaragoza, pp. 113–125.
- Salas, R., Casas, A., 1993. Mesozoic extensional tectonics, stratigraphy, and crustal evolution during the Alpine cycle of the Eastern Iberian basin. *Tectonophysics* 228, 33–55.
- Salas, R., Guimerà, J., 1997. Estructura y estratigrafía secuencial de la cuenca del Maestrazgo durante la etapa de rift jurásica superior–cretácica inferior (Cordillera Ibérica Oriental). *Boletín Geología. Y Minería* 5, 393–402 (08-4 y).
- Salas, R., Guimerà, J., Mas, R., Martín-Closas, C., Meléndez, A., Alonso, A., 2001. Evolution of the Mesozoic Central Iberian rift system and its Cenozoic inversion (Iberian Chain). In: Ziegler, P.A., Cavazza, W., Robertson, A.H.F., Crasquin-Soleau, S. (Eds.), *Peri-Tethys Memoir 6: Peri-Tethyan Rift/Wrench Basins and Passive Margins*, Mém. Mus. Natn. Hist. Nat., vol. 186, pp. 145–185.
- Searl, A., Fallick, A.E., 1990. Geochemistry of some Dinantian dolomites from East Fife: hydrothermal overprinting of early mixing-zone stable isotopic and Fe/Mn compositions. *Journal of the Geological Society (London)* 147, 623–638.
- Sellwood, B.W., Shepherd, T.J., Evans, M.R., James, B., 1989. Origin of late cements in oolitic reservoir facies: a fluid inclusion and isotopic study (Mid-Jurassic, southern England). *Sedimentary Geology* 61, 223–237.
- Shepherd, T.J., Rankin, A.H., Alderton, D.H.M., 1985. *A Practical Guide to Fluid Inclusion Studies*. London, Blackie and Sons, p. 239.
- Sibson, R.H., 1994. Crustal stress, faulting and fluid flow. In: Parnell, J. (Ed.), *Geofluids: Origin, Migration and Evolution of Fluids in Sedimentary Basins*, Geological Society Special Publication, vol. 78, pp. 69–84.
- Simón, J.L., 1984. Compresión y distensión alpinas en la Cordillera Ibérica oriental. PhD Thesis, Universidad de Zaragoza, p. 269.
- Simón, J.L., 1986. Analysis of a gradual change in stress regime: example from the Eastern Iberian Chain (Spain). *Tectonophysics* 124, 37–53.
- Spötl, C., Pitman, J.K., 1998. Saddle (baroque) dolomite in carbonates and sandstones: a reappraisal of a burial–diagenetic concept. In: Morad, S. (Ed.), *Carbonate Cementation in Sandstones*, Spec. Publs. Int. Ass. Sediment., vol. 26, pp. 437–460.
- Travé, A., Calvet, F., Soler, A., Labaume, P., 1998. Fracturing and fluid migration during Palaeogene compression and Neogene extension in the Catalan Coastal Ranges, Spain. *Sedimentology* 45, 1063–1082.
- Travé, A., Calvet, F., 2001. Syn-rift geofluids in fractures related to the Early–Middle Miocene evolution of the Vallès-Penedès half-graben (NE Spain). *Tectonophysics* 336, 101–120.
- Vallauré, T., Esteban, M., Díaz-Merino, C., Vicente, J.C., Mallo-García, J., Martínez del Olmo, W., 2003. Petroleum geology of the oil and gas commercial discoveries in Spanish basins: Mediterranean Sea. Abstract Book of the A.A.P.G. International Conference and Exhibition, Barcelona, pp. 98–99.
- Zwart, E.W., Tórent, J.L.R., 1994. Melting behavior and composition of aqueous fluid inclusions in fluorite and calcite: applications within the system $\text{H}_2\text{O}-\text{CaCl}_2-\text{NaCl}$. *European Journal of Mineralogy* 6, 773–786.